JOURNAL OF SPACECRAFT AND ROCKETS
Vol. 45, No. 4, July–August 2008

Hall Thruster Plume Model for Spacecraft Impingement Torque: Development and Validation

Ronald L. Corey,* John Steven Snyder,† Xenophon Price,‡ Shane P. Malone,§ and Thomas M. Randolph¶
Space Systems/Loral,
Palo Alto, California 94303-4604

DOI: 10.2514/1.35905

Space Systems/Loral has implemented the SPT-100 Hall effect thruster onto geostationary spacecraft for primary north–south station keeping, allowing substantial reductions in onboard propellant mass. Consideration of the spacecraft–thruster interactions is necessary when implementing electric propulsion thrusters onto communications satellites. Impingement of high-energy xenon ions on the spacecraft solar arrays and other large surfaces causes torques on the spacecraft that must be accounted for and controlled by the spacecraft control system. Space Systems/Loral has developed and used a model to predict the impingement torques on the spacecraft, allowing proper design of the spacecraft control system. The impingement model is based on experimental current-density and ion-energy data taken during ground testing. Accommodation-coefficient values for the surfaces being investigated were based on values taken from open literature. Predictions from the plume model were compared with flight control-system data from two Russian-manufactured spacecraft. Modifications to the model were made for current density, based on correlation with the flight torque data. This paper will compare predictions based on this model with flight data from the Space Systems/Loral-manufactured Galaxy 28 and Thaicom 4 geosynchronous commercial spacecraft. Both spacecraft are equipped with an SPT-100 subsystem to perform north–south station keeping.

Nomenclature

C_i = curve-fit coefficient
e = elementary charge, 1.6×10^{-19} C
F = force, N
f_ε = current-density distribution function
g = gravity constant at sea level, 9.8 m/s^2
j = current density, mA/cm^2
k_i = curve-fit coefficient
ke_i = curve-fit coefficient
m = mass, kg
p = normal momentum flux, N/m^2
R = distance from the thruster exit plane to a point in space, m
R_{cm} = distance from the thruster to the spacecraft center of mass, m
T = torque, N · m
$\bar{u}$ = current-weighted velocity, m/s
v = ion velocity, m/s
ε = ion energy, eV
θ = angle from the thruster centerline, deg
σ_n = normal momentum accommodation coefficient
σ_t = tangential momentum accommodation coefficient
σ_0 = normal momentum accommodation coefficient, $\phi = 0$
τ = tangential momentum flux, N/m^2
ϕ = incident angle with respect to surface normal, deg

Received 28 November 2007; revision received 5 March 2008; accepted for publication 19 March 2008.

*Mechanical Design Engineering Specialist, Propulsion Products, 3825 Fabian Way, Mail Stop G86. Member AIAA.
†Currently Senior Engineer, Propulsion and Materials Engineering Section, Jet Propulsion Laboratory, Pasadena, CA.
‡Principal Engineer, Dynamics and Controls Analysis Systems, 3825 Fabian Way, Mail Stop G76. Member AIAA.
§Currently, Engineer, Space Propulsion Branch, NASA John H. Glenn Research Center at Lewis Field, Cleveland, OH.
¶Currently, Project Element Manager, Propulsion and Materials Engineering Section, Jet Propulsion Laboratory, California Institute of Technology, Pasadena, CA.

I. Introduction

SPACE Systems/Loral (SS/L) has implemented the SPT-100 Hall effect thruster onto the spacecraft for primary north–south station keeping, allowing substantial reductions in onboard propellant mass and commensurate increased life compared with an equivalent chemical propulsion system. The SPT-100 subsystem provides impulse for on-orbit inclination and eccentricity control as well as momentum-wheel unloads. The SPT-100 subsystem consists of power electronics, a propellant feed system, and two stationary plasma thruster (SPT) modules. Each SPT module includes SPT-100 thrusters, thermal control, a gimbal assembly, and xenon flow controllers that contain solenoid valves and thermothrottles. The SPT module is shown in Fig. 1. A more detailed description of the SPT subsystem can be found in [1].

Consideration of the spacecraft–thruster interactions is necessary when implementing electric propulsion thrusters onto communications satellites. Impingement of high-energy xenon ions (approximately 300 eV) on the spacecraft solar arrays and other surfaces causes torques about the spacecraft center of mass (c.m.) that must be accounted for and controlled by the spacecraft control system. At 1 m from the thruster exit plane, both ion flux and velocity is a factor of 100 higher than neutral flux and velocity. For this reason, only ion flux is considered in the calculation of the impingement torque. The orientation of the solar arrays dominate the impingement torques on SS/L spacecraft due to their large area, long moment arms, and location in the SPT plume. The SPT gimbal will move to a positive elevation (smaller cant angle) the majority of the time to counter the disturbance roll torque generated by impingement on the solar array. The relative orientation of the thruster and solar array on an SS/L spacecraft is shown in Fig. 2, which also shows the solar array angle convention and SPT thrust vector location for a single thruster. To insure that the gimbal has adequate range of motion, the predicted impingement torques may be used to determine a gimbal mounting offset. If the thruster subsystem is not properly integrated onto the spacecraft (i.e., the thruster correctly aligned with the spacecraft c.m. to ensure adequate gimbal range for all phases of the mission, including the effect of impingement), some of the

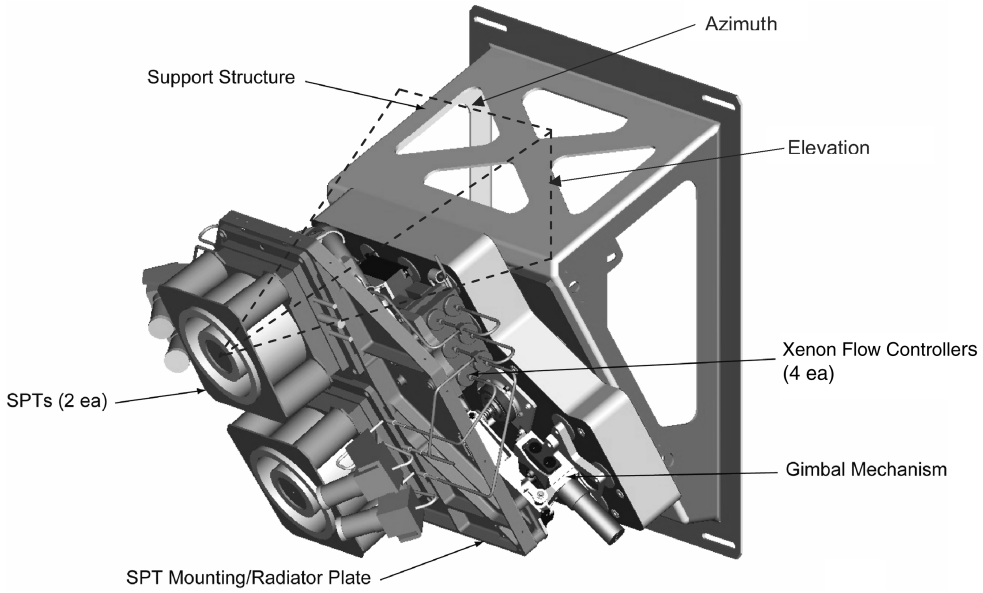

Fig. 1 SPT module showing major components.

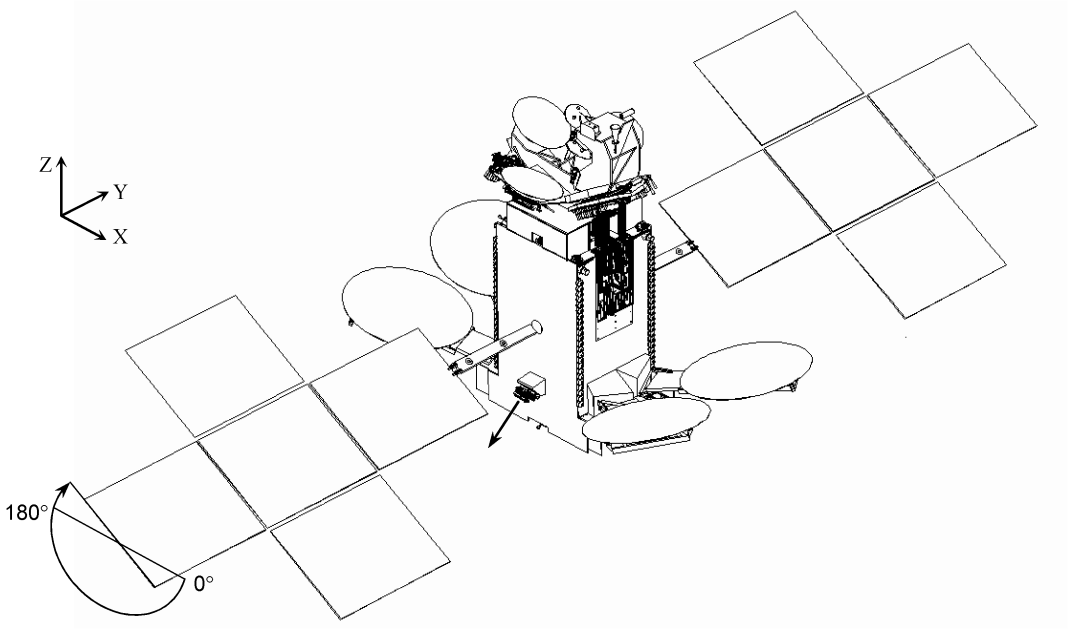

Fig. 2 Typical SS/L spacecraft showing solar array angle convention and thruster normal location.

momentum caused by the impinging thruster plume may have to be taken up by the momentum wheels. This momentum would later need to be offloaded using a chemical propulsion maneuver that would otherwise be unnecessary, which in turn reduces the spacecraft on-orbit mission life.

SS/L has developed and used a model to predict the impingement torques on spacecraft, allowing proper design of the spacecraft control operations [2,3]. The model was constructed to predict the impingement forces and torques on the spacecraft by the plume of the SPT-100 thrusters and was developed from fundamental physics principles and ground-test data. Data from the Russian Express 2A and 3A flight missions were used to benchmark the model [4–7]. This paper will compare model predictions with flight data from the Galaxy 28 (Intelsat Americas 8) and Thaicom 4 (iPSTAR 1) spacecraft.

II. Plume-Model Description

A model of the SPT plume was developed to analyze the effects of plume impingement on SS/L spacecraft. One aspect of concern is momentum flux from the plume to the spacecraft, which creates forces and torques that must be accounted for by the spacecraft control system. Momentum flux is caused by the flow of energetic particles that impinge on spacecraft surfaces. This flux is described by the rate at which the particles arrive (i.e., the plume current density), the energies that they have (i.e., the ion-energy distribution function), and the fraction of their momentum that is transferred to the spacecraft upon impact (i.e., the accommodation coefficient). The development of expressions for each of these terms and how they are used to calculate the forces and torques on the spacecraft are discussed in the following sections.

The model described herein uses fundamental physical principles combined with extensive ground-based plume measurements to predict effects on spacecraft surfaces. Hence, there are uncertainties inherent in the predictions of the model that result largely from experimental uncertainties and from the differences in plume behavior between laboratory facilities and space. The advantages of this type of model compared with more complex, completely numerical, models [8] are the transparency of the physics incorporated, rapid calculation turnaround, and ease of use. The

major disadvantages are a less rigorous treatment of the physics and a difficulty in extrapolating ground-based results to space. Although more complex models can be tremendously useful and powerful, they are affected by uncertainties related to boundary conditions and plasma parameters and their validation is subject to experimental uncertainties in ground- and space-based tests.

A. Current-Density Model

A simplifying assumption of the model is that the dependence of beam current density on the distance from the thruster is separable from the dependence on angle from the thruster centerline (and that both are separable from the ion-energy spectrum, discussed later). Description of the behavior of beam current density with the angle from the thruster centerline is taken directly from experimental measurements made 1.0 m from the thruster exit plane. Shown in Fig. 3 is a selection of beam current-density data in the plume of the SPT-100, measured at The Aerospace Corporation (TAC) and NASA John H. Glenn Research Center at Lewis Field (GRC). The GRC facility measured 4.6 m in diameter by 19.5 m in length and was able to maintain a 2.5×10^{-6} torr while the thruster was operational, and the TAC facility measured 2.4 m in diameter by 9.8 m in length and was able to maintain 4×10^{-6} torr while the thruster was operational. The probes used to take the measurements at TAC are described in [9], and the probes used to take the GRC data are described in [3]. A curve fit to the beam current-density data is also shown in Fig. 3. Unmodified TAC data alone are used for values past 90 deg. Although the GRC data set did have data out to 100 deg, it was not used, due to issues in generating the curve fit. For plume angles larger than 140 deg, it was assumed that the current density was zero. This is consistent with the data taken by King [10] that shows a negligible amount of current collected past 140 deg, with the value changing less than 1×10^{-3} mA/cm^2 from 140 to 180 deg.

Note that the data and curve fit of Fig. 3 do not accurately represent expected beam profiles in space, due to the finite pumping speeds of the vacuum chambers in which the data were acquired. The higher background pressures in ground-based facilities affect the measured Hall thruster plume properties [11]. The presence of the background gas causes a higher rate of charge-exchange collisions (CEX), making the measured current density at high angles from the thruster centerline greater on the ground than on orbit, and also causing a higher rate of momentum-exchange collisions, which results in high-energy particles being scattered to large divergence angles and reduced beam current on the plume centerline [12]. These thruster facility interactions affect the total current measured by a probe, leading to a higher measured value of the current density at large angles from the thruster centerline.

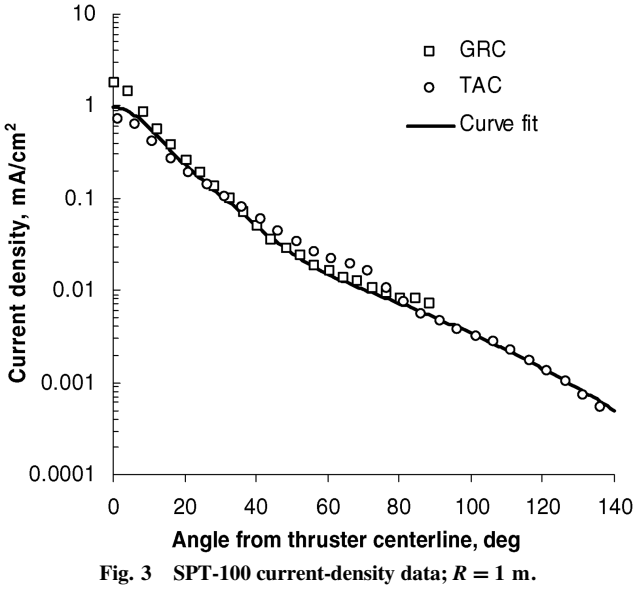

Fig. 3 SPT-100 current-density data; $R = 1$ m.

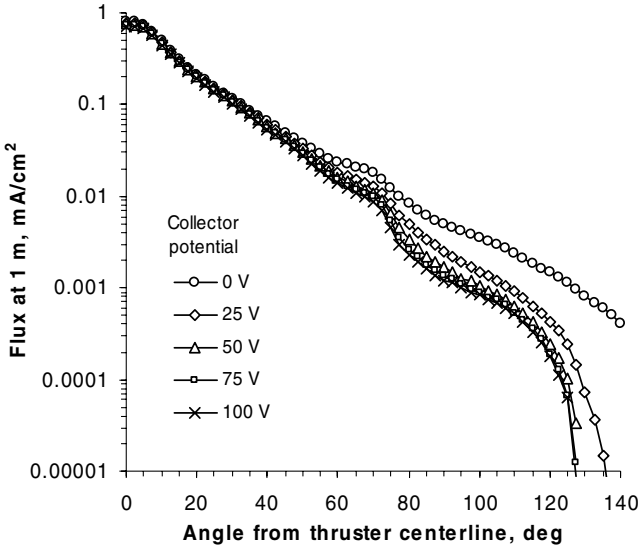

Fig. 4 Ion flux at 1 m from the thruster at various grid voltages (note the 0-V data were used in the model).

An estimate of the magnitude of the total current in the plume wings caused by CEX and scattered ion flows due to background neutrals can be determined by using a gridded flux probe [9] which rejects ions with different energy classes. To characterize these effects, current-density measurements are taken with the grid potential varied from 0 to 100 V in 25-V increments, and the data are shown in Fig. 4. At 0 V, all ion current is collected, and at 25 V, most CEX ions are screened out to approximate the in-space operating condition (although most of the CEX ions were facility-induced, there will still be some in space because of neutral efflux from the thruster). The difference in values between the 0 and 25 V data sets is significant at large angles from the thruster centerline, with a factor-of-2 difference at 90 deg. These current-density data at different screened potentials bound the error of increased ion collection at large angles, due to the presence of a background gas. Within the core of the plume, measured beam current densities will be smaller than actual due to charge-exchange reactions. Using a simple first-order approximation [11] in these tests, it was estimated that 6% of the beam ions have charge-exchange reactions within 1.0 m of the thruster.

Description of beam current density as a function of distance from the thruster is modeled using a simple spherical expansion relationship, which results in a $1/R^2$ scaling relationship for current density. Use of the $1/R^2$ assumption is desirable because it results in a simple model that is easy to apply rapidly for many applications. The accuracy of this assumption is gauged by comparison of data sets taken at similar operating conditions at two different distances from the thruster: 0.5 and 1.0 m. These data sets, scaled by $1/R^2$ to each other, are shown in Fig. 5.

Inspection of the results of Fig. 5 shows that the $1/R^2$ approximation gives very good agreement between 15 and 65 deg from the thruster centerline for both distances. At angles less than 15 deg, the current density does not scale as well. Note that the errors in current density at angles less than 15 deg are not significant for force and torque modeling, because there are no spacecraft surfaces in this portion of the plume. Greater differences are observed at angles in excess of 65 deg from the thruster centerline, from which the current density is overpredicted when scaling to a smaller distance and is underpredicted when scaling to a larger distance. The same conclusions are drawn from scaling comparisons with data acquired at 1.5 m (not shown in Fig. 5). Uncertainties in the expansion model at these larger angles are important to consider because there are spacecraft surfaces in this portion of the plume. The difference in using the spherical scaling approximation to adjust from 1 to 0.5 m is a factor of 1.4 (overpredicting current density at $\theta = 80$ deg), compared with the measurement at 0.5 m, and the difference in value going from 1 to 1.5 m is a factor of 0.6

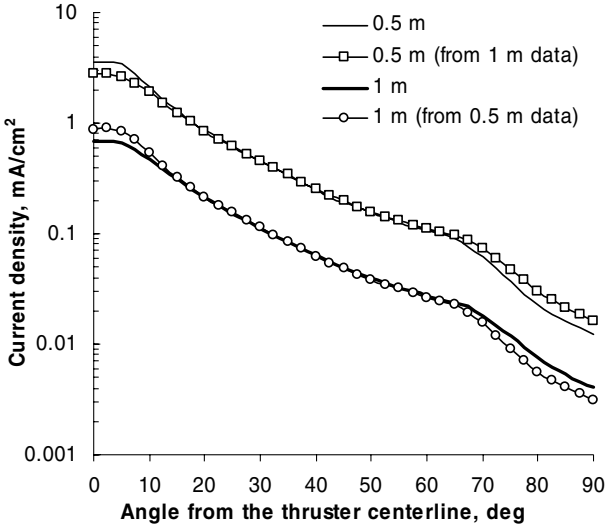

Fig. 5 Results of correcting current-density data.

(underpredicting current density at $\theta = 90$ deg), compared with the measurement at 1.5 m.

The observed deviations from the $1/R^2$ approximation are likely due to collisional effects [13]. The plume is believed to be largely collisionless, but the few collisions that do occur scatter ions from the high-density central portion of the plume out to the wings; thus, even though the fraction of scattered ions from the central beam is small, the magnitude is large when compared with the low-density regions of the plume wings. This effect was not taken into account for any of the data sets, and the resulting current density is scaled by $1/R^2$ in the final plume model. Hence, for angles greater than 65 deg, the current density is underpredicted within 1 m of the thruster and is overpredicted beyond that. (Note that there are few, if any, spacecraft surfaces within 1 m of the thruster.) Angles of less than 15 deg are not encountered in this application of the plume model, and so differences between the model and data shown in Fig. 5 do not impact the final results.

As an additional example of the accuracy of the spherical expansion model, consider data from the Express 2A and 3A satellites [4–7], shown in Fig. 6. All Express data points except those shown at 76 deg were collected by a probe fixed on the solar array that had distances from the thruster ranging from 1.4 to 9.1 m and were scaled to 1.0 m. The data points at 76 deg were collected by a probe fixed to the payload structure at a distance of 1.4 m from the thruster.

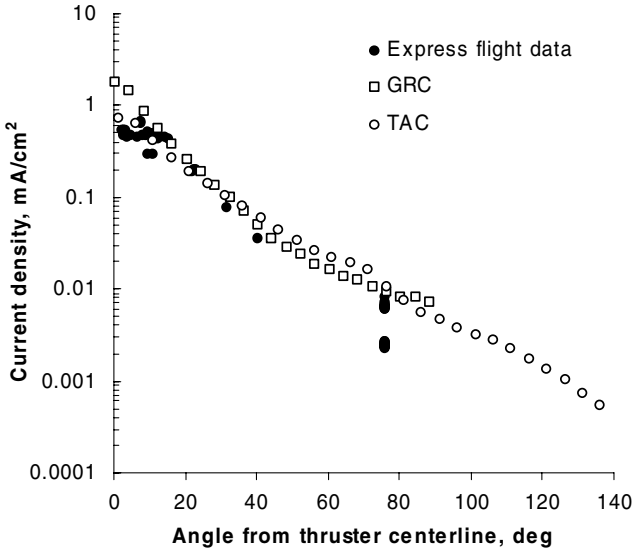

Fig. 6 Results of correcting current-density data.

Note that the majority of the data agree well with the ground-based data.

Considering the preceding discussion in this section, assigning a reasonable value for the overall uncertainty in the current-density model at every point in the plume is difficult and nearly a qualitative effort. From Fig. 3, there is a maximum variation between the three data sets of 50%. Again, these data were taken at different facilities and with different instruments. Both the uncertainty due to CEX, which is really a function of facility operation, and the $1/R^2$ scaling lead to uncertainty as a function of angle from the thruster centerline. As discussed previously, the uncertainty in using the $1/R^2$ approximation for modeling purposes is up to a factor of 0.6 (less than one, because it is underpredicted), and the difference in current-density value due to CEX was estimated to be a factor of 2 (greater than one, because it is overpredicted). However, the most important portion of the plume for modeling SS/L spacecraft is from 35 to 65 deg, with the nearest large surface (solar array panel) at $\theta = 65$ deg. At this point in the plume, the uncertainty due to CEX is 1.3, and from $1/R^2$ scaling, it is 1.05. If it is assumed that the errors stack up in a worst-case fashion, then the uncertainty could be as high as 1.4, overpredicting current density at $\theta = 65$ deg. Note that this estimate of model uncertainty is performed based on data taken from 0.5 to 1.5 m from the exit plane, and the solar array panel is 2.5 to 14.5 m from the exit plane on SS/L spacecraft.

B. Ion Energy

The plume model assumes that ion energies are a function only of angle from the thruster centerline and that they are determined from experimental measurements made 1.0 m from the engine. The ion-energy data used in the plume model were taken at The Aerospace Corporation using a retarding potential analyzer (RPA), which is described in [9]. An RPA has a sensor and a screen grid and measures the current collected as a function of screen grid potential, also known as the retarding potential. The derivative of this raw data gives the result shown in Fig. 7, which is proportional to the ion-energy distribution function. The ion-energy distribution data are shown as a function of angle from the thruster centerline. The left axis of the plot shows the differential flux ($\mathrm{mA/cm^2/V}$), and the bottom axis gives the energy per unit charge (eV), because the probe cannot distinguish between singly and multiply charged ions.

To calculate the impingement force on a given spacecraft surface, the total flux of ions must be summed over all energies. The development of the required expression begins with a monoenergetic ion flow impinging normal to a surface in which the momentum flux (or pressure) p can be defined as shown in Eq. (1):

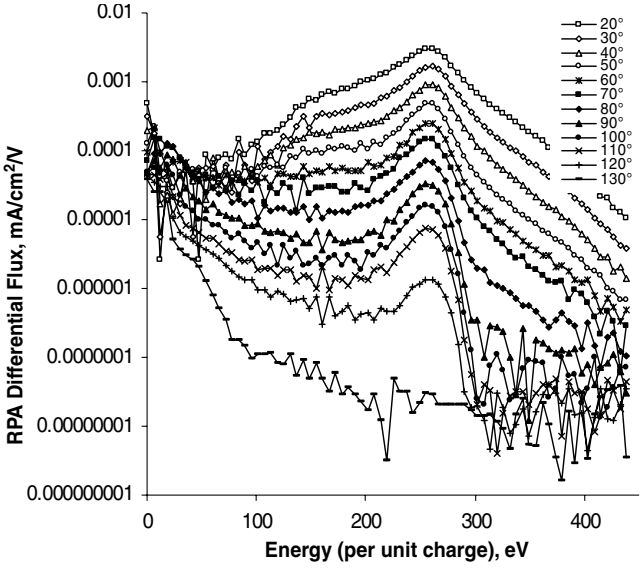

Fig. 7 Ion-energy distribution for several angles from the thruster centerline, θ.

$$p = mv\frac{j}{e} \tag{1}$$

If there is a distribution of velocities, the pressure on the plate due to a small group of ions that have velocity v can be calculated as shown in Eq. (2):

$$\mathrm{d}\,p = \frac{m}{e} v\,\mathrm{d}j \tag{2}$$

The fractional current on the plate of ions with velocity v is given by $\mathrm{d}j$. The total pressure on the plate will then be given by integration of current over all velocities, as shown in Eq. (3):

$$p = \int \mathrm{d}p = \frac{m}{e}\int v\,\mathrm{d}j \tag{3}$$

The integration over current can be performed directly from the RPA test data if the terms in the integrand are written in terms of energy:

$$p = \frac{m}{e}\int \sqrt{\frac{2e\varepsilon}{m}}\,\frac{\mathrm{d}j}{\mathrm{d}\varepsilon}\,\mathrm{d}\varepsilon \tag{4}$$

The absolute flux dependence can be removed from the integrand by substituting the normalized current-density distribution function:

$$f_\varepsilon = \frac{1}{j}\,\frac{\mathrm{d}j}{\mathrm{d}\varepsilon} \tag{5}$$

where

$$j = \int \frac{\mathrm{d}j}{\mathrm{d}\varepsilon}\,\mathrm{d}\varepsilon \tag{6}$$

Substituting for $\mathrm{d}j/\mathrm{d}\varepsilon$ in Eq. (4) gives Eq. (7):

$$p = j\frac{m}{e}\int \sqrt{\frac{2e\varepsilon}{m}} f_\varepsilon \mathrm{d}\varepsilon \tag{7}$$

Note that the integrand in Eq. (7) is a velocity term [compare with Eq. (3)].

Equation (7) is a simple equation for calculating the pressure on a plate from an ion flux normal to the surface. To ease the interpretation of Eq. (7) and to write it in terms that make plume-analysis calculations convenient, the current-weighted velocity $\bar{u}$ is defined:

$$\bar{u} \equiv \int \sqrt{\frac{2e\varepsilon}{m}} f_\varepsilon \mathrm{d}\varepsilon \tag{8}$$

The current-weighted velocity is easily calculated directly from the RPA data:

$$\bar{u} = \int \sqrt{\frac{2e\varepsilon}{m}} f_\varepsilon\,\mathrm{d}\varepsilon = \int \sqrt{\frac{2e\varepsilon}{m}}\,\frac{1}{j}\,\frac{\mathrm{d}j}{\mathrm{d}\varepsilon}\,\mathrm{d}\varepsilon = \frac{\int \sqrt{(2e\varepsilon/m)}(\mathrm{d}j/\mathrm{d}\varepsilon)\,\mathrm{d}\varepsilon}{\int(\mathrm{d}j/\mathrm{d}\varepsilon)\,\mathrm{d}\varepsilon} \tag{9}$$

where the calculation can now be performed directly from the RPA ion-energy data. Note that Eq. (9) assumes that only singly charged ions are present. Note also that because the current-density distribution function $\mathrm{d}j/\mathrm{d}\varepsilon$ is a function of angle from the thruster centerline, the current-weighted velocity will also be a function of angle, as shown in Fig. 8. Also note that Eq. (9) is not an average velocity. To calculate the average velocity, one would have to use the number-density distribution function $\mathrm{d}n/\mathrm{d}\varepsilon$ instead of the current-density distribution function $\mathrm{d}j/\mathrm{d}\varepsilon$ in Eq. (9). The difference between the number-density and current-density distributions is the charge state.

Performing the calculation in this manner introduces an uncertainty that is difficult to quantify, because Eq. (1) assumes that all ions are singly charged. Double ions with the same E/q as singles have twice the energy and thus transfer more momentum to a surface. The RPA data do not distinguish between charge states.

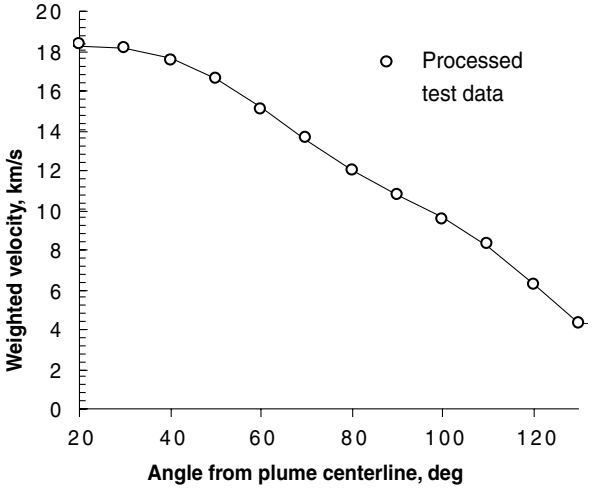

Fig. 8 Current-weighted velocity.

However, charge state data were taken using a time-of-flight device described in [9]. These data show that, on average, between 20 and 90 deg from the plume centerline, the plume is 76% singles, 19% doubles, 5% triples, and 1% quadruples. The complete data set is shown in Table 1.

From Table 1, it is clear that assuming that the plume is primarily made up of singly charged ions is not valid. In reality, the energy would be underpredicted in 19% of the plume by $\sqrt{2}$, in 5% of the plume by $\sqrt{3}$, and in 1% of the plume by $\sqrt{4}$. This would lead to an overall uncertainly of 13%, and thus the model may underpredict momentum by a factor of 1.13. Note that this is an approximation, because the multiply charges ions are not necessarily evenly distributed across all velocities.

C. Accommodation Coefficients

Momentum transfer from the individual plume particles to the spacecraft is modeled using the accommodation coefficients. The normal and tangential accommodation coefficients σ_n and σ_t are defined to have values between 0 and 1, with an accommodation coefficient of 1 (meaning that an atom colliding with a surface transfers all of its momentum to the surface in both the tangential and normal directions) and an accommodation coefficient of 0 (meaning that the atom rebounds perfectly from the surface, transferring twice its normal momentum, but none of its tangential momentum). The normal and tangential accommodation coefficients are defined as follows:

$$\sigma_n = \frac{p_i - p_r}{p_i - p_s} \tag{10}$$

$$\sigma_t = \frac{\tau_i - \tau_r}{\tau_i} \tag{11}$$

where p is the normal momentum flux, τ is the tangential momentum flux, subscripts i and r indicate incident and reflected components, and p_s is the normal momentum flux of the gas if it was reflected diffusely at surface temperature [14].

Table 1 Ion species distribution at 1 m from the thruster exit plane

Angle	Single, %	Double, %	Triple, %	Quadruple, %
20	76.6	14.9	7.1	1.4
30	71.3	20.6	7.4	0.7
40	67.7	25.5	5.6	1.2
50	77.5	18.8	3.2	0.5
60	80.5	16.1	3.4	
70	79.2	17.0	3.8	
80	79.8	16.9	3.4	
90	77.6	18.3	4.1	
Average	76.3	18.5	4.8	1.0

Table 2 Normal momentum accommodation coefficients at normal incidence

Target material	σ_0	Reference
Al	0.9	[18]
Si	0.94	[18]
Ti	0.88	[18]
Ni	0.84	[18]
W	0.65	[18]
Quartz	0.825	[17]
Stainless steel	0.62	[18]
Al dia (aluminized polymer film with glass mesh)	0.86	[16]
Al poly (aluminized polymer film)	0.84	[16]
AK512 (white enamel)	0.8	[17]

The value of the accommodation coefficients can vary, depending on many different factors, including incoming ion type, surface type, surface roughness, surface temperature, incident angle, and incoming ion energy. In general, the kinetic energy of ions incident onto a surface is transformed into vibration energy of the atoms inside the solid. The size of this energy loss depends on the penetration of the ions into the solid. Other phenomena such as sputtering, electron emission, and desorption also produce an energy loss of the incident ions. For metal targets, the accommodation coefficients increase with increasing energy, which can be explained by assuming that the particles penetrate progressively deeper into the solid as their kinetic energy increases. The accommodation coefficients decrease as the angle of incidence increases, because the atoms do not penetrate as deeply into the surface and therefore the energy lost by the impinging atom is not as large [14,15]. A literature search was performed to determine reasonable values for the accommodation coefficients [16–18] of xenon ions on typical SS/L spacecraft surface materials. The references found do provide data for xenon ion impingement on surfaces; however, the data do not exactly match the ion velocities or materials used (except for quartz) for the specific SPT-100 and spacecraft model presented.

Table 2 and Fig. 9 show a summary of values found in the literature for xenon impinging onto a surface. Incident ion energies are 70 eV for all data shown. The surface labeled Al poly is for an aluminumized polymer film. The surface labeled Al dia is an aluminumized polymer film with a conductive surface covered with a glass mesh that has a transparency of 0.12. The surface labeled AK512 is a white enamel. References [16–18] are concerned primarily with low-Earth-orbit satellite drag, and so most data presented are for nitrogen impingement onto a surface. However, an empirical expression for the normal accommodation coefficient for xenon impingement onto a surface was given and justified in [16].

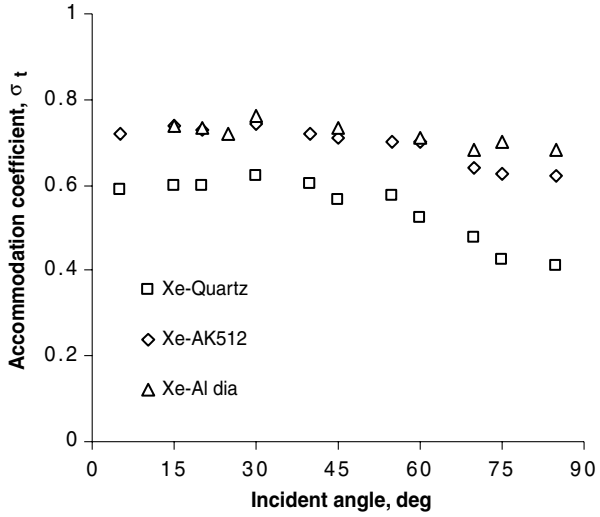

Fig. 9 Tangential momentum accommodation coefficients.

The empirical fit is shown in Eq. (12):

$$\frac{\sigma_n}{\sigma_0} = \cos^{\frac{3}{5}}\phi + \frac{a_1 \sin^2\phi}{1 + \frac{1}{\sigma_0}} \tag{12}$$

where $a_1 = 0.846$ for xenon. This equation is assumed to be valid for all surfaces shown in Table 2. The SS/L solar array consists of quartz-covered solar cells bonded to a carbon-fiber mesh substrate. The data given for quartz combined with Eq. (12) are used directly in the model for σ_n for the front side of the array. The back side of the solar array has a complex surface topography, as does the Xe-Al-dia surface given in the literature. Therefore, for the back side of the solar array, a constant value of 0.74 was assumed for σ_t, based on the Xe-Al-dia surface data, which are nearly constant as a function of angle. For σ_n, only normal incident data were given for Xe-Al dia. Because of a lack of data for both the solar array construction (for the Russian Express satellites) and xenon ion impingement onto such a surface (or for the SS/L spacecraft surface), a constant value of 0.9 was assumed for σ_n. The author of [15] states that the uncertainty in measuring the accommodation coefficient is ± 0.05. However, because the data used do not match the ion velocities or materials used (except for quartz), the error is probably greater than this. Note that quartz is the more specular surface and so will be the biggest contributor to impingement torque.

D. Calculating Forces and Torques

The normal and tangential momentum fluxes (pressure and shear force) are determined from the current density, ion-energy distribution, the plume geometry, and the accommodation coefficients. Note that the current-density values are calculated from the 1-m values scaled by $1/r^2$ to the location of the spacecraft, and the ion-energy distributions have no dependence on distance. The normal momentum flux is given by Eq. (13), and the tangential momentum flux is given by Eq. (14):

$$p(r,\theta,\phi) = (2 - \sigma_n)\frac{m}{e}\bar{u}(\theta) j(r,\theta)\cos\phi \tag{13}$$

$$\tau(r,\theta,\phi) = \sigma_t \frac{m}{e}\bar{u}(\theta) j(r,\theta)\sin\phi \tag{14}$$

From the tangential and normal momentum fluxes, the forces in three orthogonal spacecraft axes are determined at each calculation-grid location on the spacecraft. The plume model takes a 3-D CAD model as input and automatically calculates the relevant geometric parameters for a given grid location on the spacecraft, including the distance from the thruster to the cell, r, the angle from the thruster centerline to the cell, θ, the incidence angle on the cell, ϕ, and the distance from the grid location to the spacecraft c.m., R_{cm}. To easily use the current-density and current-weighted velocity terms in the model, the following curve-fit forms were used:

$$j = \frac{R^2}{r^2}\left(k_0 \exp\left(-\left(\frac{\theta}{k_1}\right)^{ke_0}\right) + k_2 \exp\left(-\left(\frac{\theta}{k_3}\right)^{ke_1}\right) + k_4 \exp\left(-\left(\frac{\theta}{k_5}\right)^{ke_2}\right)\right) \tag{15}$$

$$\bar{u} = \sum_{i=0}^{7} C_i \theta^i \tag{16}$$

Note that Eqs. (15) and (16) are defined for $\theta \leq 140$ deg.

The impingement torques can then be calculated using Eq. (17):

$$\vec{T} = \vec{F} \cdot \vec{R}_{\text{cm}} \tag{17}$$

where $F = p$ (or τ) multiplied by the grid area.

In Secs. II.A–II.C, an attempt was made to quantify the uncertainty for the current density, ion energy, and accommodation coefficients. From Eqs. (13) and (14), these three quantities are linearly

dependent; therefore, the uncertainties for each quantity can be multiplied to yield a total uncertainty for the calculation. Each section lists a significant uncertainty: not only measurement uncertainty, but also uncertainty in comparing ground data with in-space operation. From the error analysis discussed in each section (1.4 for current density, 1.13 for energy, and 1.05 for accommodation coefficient), if all uncertainties are root-sum-squared, there is a factor of 1.37 total model uncertainty at $\theta = 65$ deg. Even with access to a 3-D numerical code, it seems unlikely that a rigorous analysis could be performed to exactly gauge the uncertainty in each quantity to provide for corrected values for input into the model.

A simple ground-based experiment was performed to assess a limited portion of the uncertainty in the plume model that is due to the assumptions and approximations used in the current-density, ion-energy, and accommodation-coefficient models. A standard SS/L flight solar array coupon was mounted onto a precision thrust stand and placed at a distance of 0.6 m from the exit plane of an SPT-100 at an angle of 30 deg from the centerline. This test was performed at The Aerospace Corporation in the same facility and with the same thruster used to obtain the plume data discussed in Secs. II.A and II.B. The coupon was rotated through a full 360-deg circle while the impingement force was recorded, exposing both the coupon cover glass and backing material to the plume. The results of this test are compared in Fig. 10 with the plume-model calculations. Excellent agreement is seen between test and model for all but the near-orthogonal data, which were likely affected by local pressure increases near the coupon face in this high-density region of the plume. Although this comparison does not address the uncertainties in the plume model related to the difference between plume behavior in space and in ground-based facilities, it demonstrates that the model formulation is appropriate to describe the observed behavior and that the selection of accommodation-coefficient values for the flight coupon is also appropriate.

III. Flight Data

Flight data are presented for the Russian Nauchno-Proizvodstvennoe Obiedinenie Prikladnoi Mekhaniki (NPO-PM)-manufactured Express 2A and 3A spacecraft and for the SS/L-manufactured Galaxy 28 and Thaicom 4 spacecraft. The Express 2A and 3A spacecraft measured the plume impingement at various solar array angles by noting the reaction torques of the attitude control system while the thrusters were fired. The spacecraft telemetry used to calculate impingement torque on the SS/L-manufactured spacecraft is the solar array angle and the gimbal-actuator step count. The gimbal data presented were converted from step count to gimbal elevation and azimuth angles. The plume model was first benchmarked by comparison with the Express data and then compared with the SS/L flight data.

A. Fit to Russian Flight Data

The SS/L impingement-torque plume model was configured with the Express geometry and the current-density data, ion-energy data, and accommodation-coefficient data previously discussed, which was used to compare with the Express 2A and 3A flight data [4–7] to benchmark the plume model. The Express 2A and 3A spacecraft measured the plume impingement at various solar array angles by noting the reaction torques of the attitude control system while the thrusters were fired. The Express momentum-wheel torque-data error was assumed to be negligible. It is SS/L's experience that wheel speed measurements are reliable. The main errors that exist are in modeling the Express spacecraft geometry (because no 3-D CAD model was available) and in determining the correct surface-material properties. Because of this, only the Express solar array, yoke, radiator and a truncated cone representing the payload were modeled. Other surfaces that protrude into the plume were not modeled, but their effects are still present in the wheel data. The error, however, is likely small, because the payload structure lies beyond 80 deg from the plume centerline. Hence, the solar array is, by far, the dominant source of impingement torque on the spacecraft, because it lies between 15 and 40 deg from the plume centerline. An additional small source of error is due to the greater uncertainty in the plume-model data at angles less than 20 deg from the thruster centerline. This error is not expected to have a significant effect on the results, because the impingement torque is typically dominated by the surfaces nearer to the thruster (i.e., larger plume angles) for these types of spacecraft geometries.

Flight data from these spacecraft are shown in Figs. 11–14. Considering the significant uncertainties in the plume and spacecraft models, there is good agreement between the flight data and plume model. It is possible that these results are fortuitous because of the uncertainties associated with modeling the Express spacecraft and interpreting the flight data. It is interesting to note that the Express data indicate that the front and back sides of the solar arrays have different values for the accommodation coefficients, as was noted in Sec. II.C. It can be inferred from the data that the back side of the array (shown as 0–180 in Figs. 11–14) is more diffusive than the front side of the array (shown as 180–360 in Figs. 11–14). The Express solar array is made of an aluminum frame covered with fiberglass to which the solar cells attach. The plume model assumes that this panel is solid. Given that the solar array front side is mostly glass and the back side is of rough construction, the more specular nature of the front side seems reasonable. As can be seen from Figs. 11–14, there was fairly good agreement with the Express data and the plume model without any modification to the plume model. Agreement with the model for the Z axis (not shown) was not as good as for the other

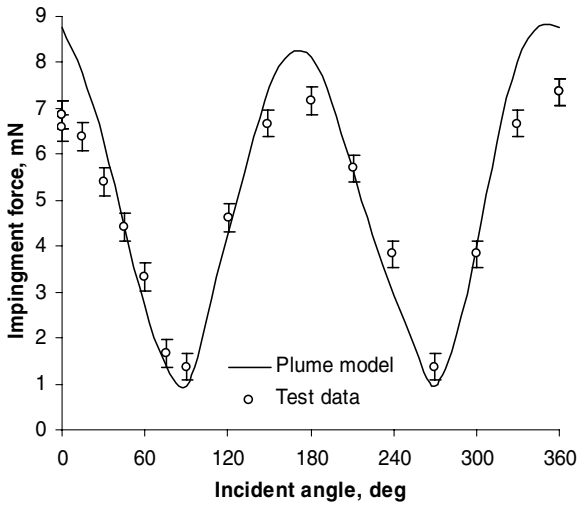

Fig. 10 Impingement-force measurements on a flight-design solar array coupon in an SPT-100 plume.

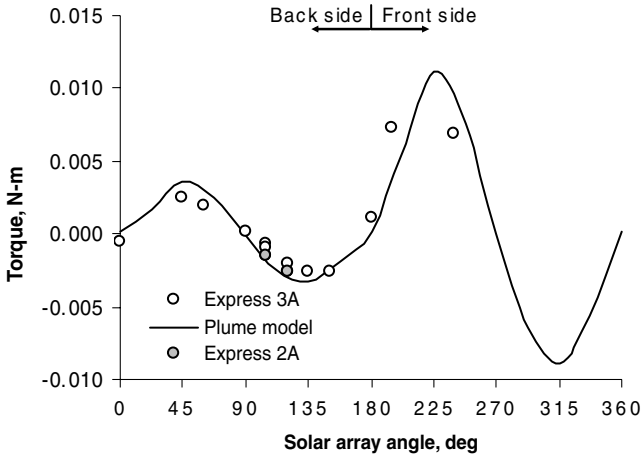

Fig. 11 Plume-model impingement-torque prediction for Express thruster RT4 *X* axis.

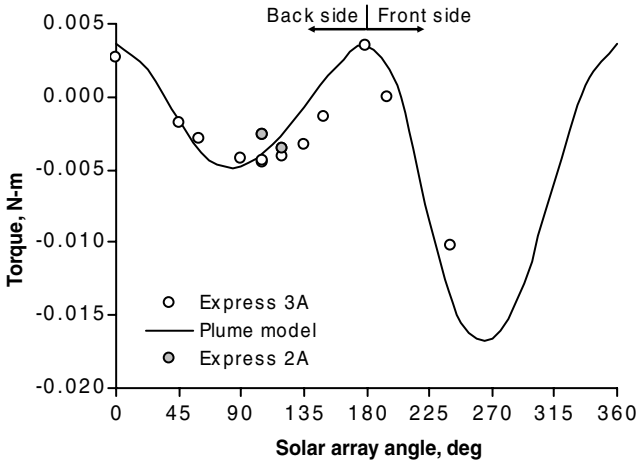

Fig. 12 Plume-model impingement-torque prediction for Express thruster RT4 *Y* axis.

Fig. 13 Plume-model impingement-torque prediction for Express thruster T4 *X* axis.

axes, likely because the torque measured in this axis was about an order of magnitude less than in the other axes, and hence the uncertainties in the measurement were more significant.

These results seem to indicate that the difference between the plume behavior in space- and ground-based facilities are minor in the range of the Express solar arrays (i.e., 12 to 45 deg from the thruster centerline and 3.8 to 10 m from the thruster exit plane). The ground-based plume data indicate that uncertainties (for example, due to the $1/R^2$ scaling and scattering and CEX effects) are small in this region. There are some protruding features on the Express spacecraft that lie in the 80-deg-or-greater portion of the plume, but this is a small area compared with the area of the solar array. When using this Express spacecraft benchmarked model to predict impingement torque on SS/L spacecraft, it is important to note that the geometries are quite different. As can be seen in Figs. 1 and 2, the SS/L configuration is such that the solar array lies in the 35- to 65-deg portion of the plume, and there is a significant area below the thruster at plume angles of 70 deg or greater. In other words, the particular geometry of SS/L spacecraft is such that large areas of the spacecraft are in regions in which the uncertainties in the plume model are larger than for the Express.

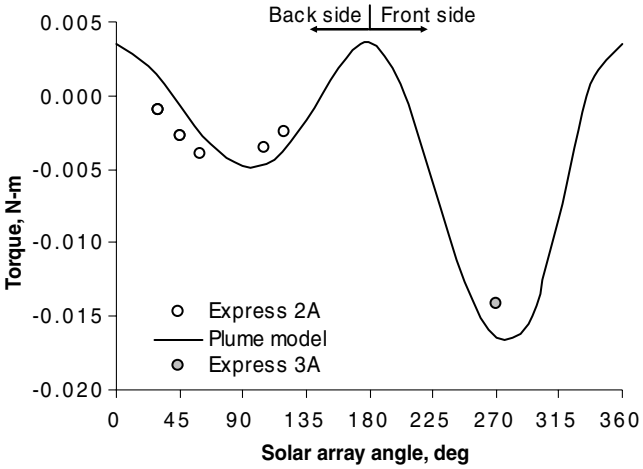

Fig. 14 Plume-model impingement-torque prediction for Express thruster T4 *Y* axis.

B. Galaxy 28

The Galaxy 28 (G28) spacecraft launched on 23 June 2005 from a sea launch (154° west longitude, 0° latitude). The data presented for this spacecraft were taken from the thruster in-orbit testing following the final insertion into the orbital slot. On G28, a plume torque test was performed in which a north-side thruster was fired eight times for 1.5 h each time, over a 24-h period. The gimbal angle and solar array angle conventions for SS/L flight data are shown in Figs. 1 and 2, respectively. The G28 spacecraft has the smallest cant angle with respect to the solar array of the SS/L spacecraft data presented. For all SS/L spacecraft data shown in which the model is matched to flight data, the offset to the curves were matched by the addition of constants. This is done for presentation purposes to more easily show a visual comparison of the model vs the actual data. This offset is due mainly to the actual-vs-predicted spacecraft center-of-mass values for the satellites and, in practice, it manifests itself as a fixed offset in the gimbal position. Note that this offset is not related to an error or uncertainty in the plume model, but rather from uncertainty in determining the mass properties of the spacecraft as delivered to its orbital position. Error bars shown on the data represent gimbal hysteresis, diurnal motion of the xenon in the tanks (tanks share a common manifold), and spacecraft thermal distortion. Note that G28 and Thaicom 4 were launched with different xenon loads, and so these error bars are different for each spacecraft.

The eight data points shown in Fig. 15 were taken at the end of each burn and reflect the final gimbal positions. The data were taken at the end of the SPT firing, because the force imparted on the spacecraft by the thruster causes the bipropellant to move in the tanks,

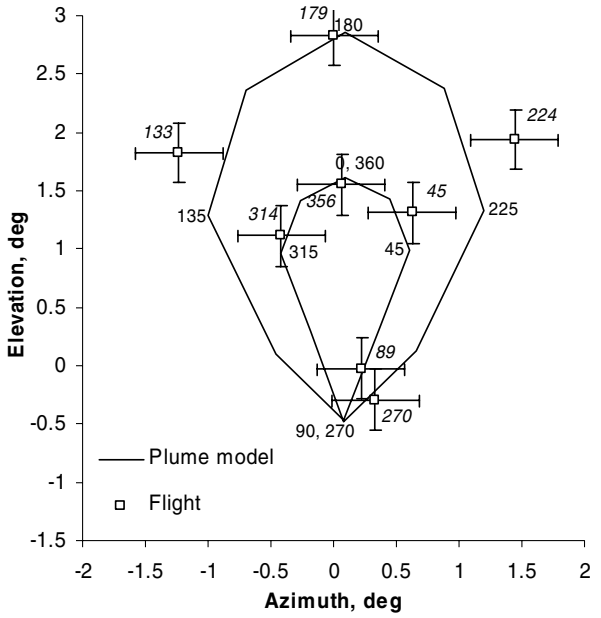

Fig. 15 Azimuth vs elevation angle for the G28 spacecraft as a function of solar array angle (values listed are for the model, and italic values are for the measured flight).

changing the spacecraft c.m.. It takes approximately 1 h for the spacecraft c.m. to reach equilibrium during the firing. Each burn shown in Fig. 15 was approximately one-and-a-half hours in duration. Initial comparison of the flight data with the plume-model predictions showed that although the trends were accurately predicted, the magnitude of the calculations was approximately a factor of 2 lower than the flight measurements. This multiplier was applied to the end result of the calculation; to which term of the equation the factor applies (e.g., current density, energy, or accommodation coefficients) cannot be distinguished. Figure 15 shows the plume model adjusted by a factor of 2 and compared with the flight data.

Considering the agreement between the Express flight data and plume-model calculations, the factor-of-2 difference in the SS/L flight data is greater than anticipated. The difference is possibly related to the spacecraft configuration, as discussed previously. The Express solar array was closer to the plume centerline, from which there is less error in determining the plume current density. Also, there is not a large area close to the thruster in the opposite direction of the solar array, as is the case for $\pm Y$ panels on SS/L spacecraft, as shown in Fig. 2. To differentiate these two effects, the plume model was run with only the G28 solar array and not the Y panel. Elimination of the lower panel in the model eliminates a constant impingement torque and should simply shift the entire plot vertically upward. It was found that modeling only the solar array still required a factor-of-1.8 increase to fit to the flight data, indicating that the effect of the panels in the model is small. The model was also run with a plume current-density profile that rejected current due to low-energy ions (i.e., the 25-V data set of Fig. 4) with the results being nearly identical. These results suggest that the bulk of the error in modeling momentum transfer to the SS/L solar array is not due to large-angle effects but to effects nearer the core of the plume (i.e., 65 deg).

C. Thaicom 4

The Thaicom 4 spacecraft launched on 11 August 2005 from Kourou, French Guiana, on an Ariane V. The data presented in Fig. 16 were taken from the thruster in-orbit testing following the final insertion into the orbital slot. On Thaicom 4, the same in-orbit plume torque test as Galaxy 28 was performed. Thaicom 4 has a cant angle that is roughly 5 deg higher than that of G28, and therefore there is less impingement force onto the spacecraft. All data presented for the Galaxy 28 and Thaicom 4 spacecraft are for the north side of the spacecraft. The plume-model data shown in Fig. 16 were calculated using the plume model with a constant factor of 2 applied. It can be seen that the Thaicom 4 data agree well with the model calculations, with the data trend accurately predicted, which indicates that plume-model predictions and correlation to flight data are relatively insensitive to minor differences in individual spacecraft geometries.

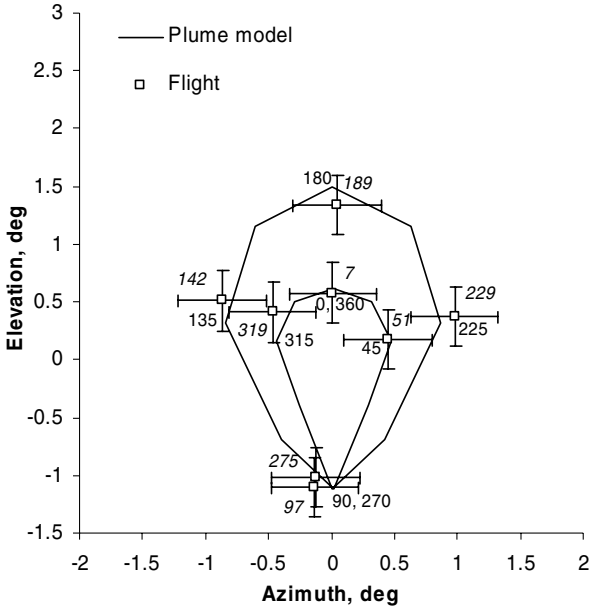

Fig. 16 Azimuth vs elevation angle for the Thaicom 4 spacecraft as a function of solar array angle (values listed are for the model, and italic values are for the measured flight).

IV. Conclusions

A simple plume model based on fundamental physics principles and data from ground-based tests was constructed and compared with flight-impingement torque data for three different spacecraft. The model is based on separable functions for beam current-density dependence on distance from the thruster, beam current-density dependence on the angle from the thruster centerline, and ion-energy dependence on the angle from the thruster centerline. The advantages of this type of model compared with more complex, completely numerical, models are the transparency of the physics incorporated, rapid calculation turnaround, and ease of use. The major disadvantages are a less rigorous treatment of the physics and a difficulty in extrapolating ground-based results to space.

The model was successfully benchmarked against ground-test data with a solar array coupon, and comparison with flight data from the Express spacecraft indicated good agreement. Significant differences were observed, however, between the plume-model predictions and flight data from two SS/L spacecraft. Model predictions of the momentum transfer effects were less than the flight data by a factor of approximately two for both spacecraft. The factor-of-2 discrepancy appears to result from uncertainties in the plume model in the region of solar array impingement (i.e., 35 to 65 deg from the thruster centerline and 2.5 to 14.5 m from the exit plane). It is difficult to assess the magnitude of the uncertainty in the SS/L plume model based on the data used to generate it, but from the information available, it seems that a factor of 2 is not unreasonable. Qualitatively, the data trends as predicted. For example, the G28 spacecraft has the smallest cant angle with respect to the solar array of the SS/L spacecraft data presented. Thaicom 4 has a cant angle roughly 5 deg higher than G28 and the flight data show the expected reduction in magnitude as the cant angle increases.

The correlation of the plume model to flight data from two SS/L spacecraft allows for accurate prediction of impingement torque onto the spacecraft surfaces for future SS/L spacecraft with designs similar to G28 and Thaicom 4. Advanced numerical models may be required for significantly more complex geometries. Although the plume model used is simple compared with a three-dimensional numerical model, it is a useful design tool. The correlated SS/L plume-impingement model allows for future spacecraft equipped with SPTs to be designed with greater confidence.

Acknowledgments

The authors would like to thank Jim Pollard of The Aerospace Corporation for taking the data used in constructing the SPT-100 plume model, Kevin Diamant of The Aerospace Corporation for taking the solar array coupon data, and Jeff Baldwin of Space Systems/Loral (SS/L) for his work constructing the SS/L plume-analysis software.

References

[1] Randolph, T., Fischer, G., Pidgeon, D., Rogers, W., Staley, M., Bekrev, M., Day, M., Koriakin, A., Kozubsky, K., Krockak, L., Maslennikov, N., Pridannikov, S., and Yuriev, A., "Integrated Test of an SPT-100 Subsystem," AIAA Paper 97-2915, 1997.

[2] Pencil, E. J., Randolph, T. M., and Manzella, D. H., "End-of-Life Stationary Plasma Thruster Far-Field Plume Characterization," AIAA Paper 96-2709, 1996.

[3] Randolph, T., Pencil, E. J., and Manzella, D. H., "Far-Field Plume Contamination and Sputtering of the Stationary Plasma Thruster," AIAA Paper 94-2855, 1994.

[4] "Hall Effect Thruster Interactions Data from the Russian Express-A2 and Express-A3 Satellites," NASA CR-2003-212005, Pt. 2, June 2003.

[5] "Hall Effect Thruster Interactions Data from the Russian Express-A2 and Express-A3 Satellites," NASA CR-2003-212005, Pt. 4, June 2003.
[6] "Hall Effect Thruster Interactions Data from the Russian Express-A2 and Express-A3 Satellites," NASA CR-2003-212005, Pt. 1, June 2003.
[7] "Hall Effect Thruster Interactions Data from the Russian Express-A2 and Express-A3 Satellites," NASA CR-2003-212005, Pt. 3, June 2003.
[8] Mikellidies, I. G., Jongeward, G. A., Katz, I., and Manzella, D. H., "Plume Modeling of Stationary Plasma Thrusters and Interaction with the Express-A Spacecraft," *Journal of Spacecraft and Rockets*, Vol. 39, No. 6, 2002, pp. 894–903.
[9] Pollard, J. E., Diamant, K. D., Khayms, V., Werthman, L., King, D. Q., and DeGrys, K. H., "Ion Flux, Energy, and Charge State Measurements for the BPT-4000 Hall Thruster," AIAA Paper 2001-3351, 2001.
[10] King, L. B., "Transport Property and Mass Spectral Measurements in the Plasma Exhaust Plume of a Hall Effect Space Propulsion System," Ph.D. Thesis, Univ. of Michigan, Ann Arbor, MI, 1998.
[11] Randolph, T. M., Day, M. L., Kim, V., Kaufman, H. R., Zhurin, V. V., and Kozubsky, K., "Facility Effects on SPT Thruster Testing," International Electric Propulsion Conference Paper 93-093, 1993.
[12] Katz, I., Jongeward, G., Davis, V., Mandell, M., Mikellides, I., Dressler, R., Boyd, I., Kannenberg, K., Pollard, J., and King, D., "A Hall Effect Thruster Plume Model Including Large Angle Elastic Scattering," AIAA Paper 2001-3355, 2001.
[13] Boyd, I. D., "Hall Thruster Far Field Plume Modeling and comparison with Express Flight Data," AIAA Paper 2002-0487, 2002.
[14] Devienne, F. M., "Variations of the Accommodation Coefficient of High Energy Molecules on Metal in Terms of Different Parameters," *4th International Rarefied Gas Dynamics Symposium*, Academic Press, New York, 1966, pp. 595–606.
[15] Devienne, F. M., Roustan, J. C., and Clapier, R., "Speed Distribution of Scattered Molecules after the Impact of a High Velocity Molecular Beam on a Solid Surface," *5th International Rarefied Gas Dynamics Symposium*, Academic Press, New York, 1967, pp. 269–288.
[16] Shuvalov, V. A., "Transfer of Gas-Ion Momentum and Energy to an Electrically Conductive Surface Partially Coated by a Thin Diaelectric Layer," *Journal of Applied Mechanics and Technical Physics*, Vol. 27, No. 4, 1987, pp. 478–485.
doi:10.1007/BF00910186
[17] Shuvalov, V. A., "Exchange of Energy and Momentum Between Ions and in a Rarefied Plasma Flow and an Electrically Conducting Surface Coated with a Thin Layer of Dielectric," *High Temperature*, Vol. 25, No. 4, 1987, pp. 477–481.
[18] Shuvalov, V. A., "Transfer of the Momentum of Gas into the Surface of a Solid," *Journal of Applied Mechanics and Technical Physics*, Vol. 25, No. 3, 1984, pp. 351–358.
doi:10.1007/BF00910392

I. Boyd
Associate Editor